Effects of laser polarizations on shock generation and shock ion acceleration in overdense plasmas

Young-Kuk Kim,[1] Teyoun Kang,[2] Moon Youn Jung,[3] and Min Sup Hur[2,*]

[1]*School of Electrical and Computer Engineering, UNIST, 50 UNIST-gil, Ulju-gun, Ulsan 689-798, Korea*

[2]*School of Natural Science, UNIST, 50 UNIST-gil, Ulju-gun, Ulsan 689-798, Korea*

[3]*Bio-Photonics Research Section, Electronics and Telecommunications Research Institute,*
218 Gajeong-ro, Yuseong-gu, Daejeon 305-700, Korea

The effects of laser-pulse polarization on the generation of an electrostatic shock in an overdense plasma were investigated using particle-in-cell simulations. We found, from one-dimensional simulations, that total and average energies of reflected ions from a circular polarization- (CP) driven shock front are a few times higher than those from a linear polarization- (LP) driven one for a given pulse energy. Moreover, it was discovered that the pulse transmittance is the single dominant factor for determining the CP-shock formation, while the LP shock is affected by the plasma scale length as well as the transmittance. In two-dimensional simulations, it is observed that the transverse instability, such as Weibel-like instability, can be suppressed more efficiently by CP pulses.

I. INTRODUCTION

Recently, the generation of an electrostatic (ES) shock and shock ion acceleration have attracted much attention as this method can generate highly energetic and quasimonoenergetic ion beams from relatively moderate (compared to the radiation-pressure-acceleration [1]) laser-pulse intensity and near-critical plasmas [2–9]. When an electrostatic shock is formed in a plasma with velocity v_{sh}, incoming ions to the shock are reflected from the shock front with $v_{ref} \sim 2v_{sh}$. The accelerated ions in this way have been expected to be used for various applications such as cancer therapy [10–12], isotope generation [13], and proton imaging [14].

One of the essential conditions for generating electrostatic shocks is the compression of a density layer, whose Mach number falls into a proper range $1.5 < M < 3.7$ [2,15], where $M = v/c_s$ and $c_s = \sqrt{ZKT_e/m_i}$ is the sound speed. Such a high-speed compression layer can be formed primarily by the hole-boring process [16,17]. Another important ingredient for shock formation is the electron heating in the upstream to obtain high-enough sound speed to be matched to the velocity of the compression layer. One way to heat electrons is to recirculate hot electrons supplied into the upstream by the oscillating ponderomotive force of a linearly polarized (LP) laser pulse [18,19]. Recent experiments have shown the generation of multi-MeV monoenergetic proton beams from electrostatic shock, where LP CO_2 laser pulses were used along with a near-critical-density gas jet [8,20].

Direct heating of the upstream electrons by transmitted laser-pulse energy is another heating mechanism. Previously, we suggested using the relativistic transparency for shock generation by circularly polarized (CP) pulses [21], where hot-electron recirculation is not available. Regarding the effects of transmittance on shock formation, there have been seemingly contradictory results; Zhang *et al.* could obtain a quasimonoenergetic carbon beam of ~7.5 MeV from an opaque plasma irradiated by an LP pulse but could not do so in transparent plasma [22]. Meanwhile, Lecz *et al.* observed that shock ion acceleration was more efficient in semitransparent plasmas with 20–30% transmittance [23]. Therefore, the effects of pulse transmittance, which acts on the shock formation in different ways depending on laser polarization, still need more investigation. In particular, the effects of circular polarization related to transmittance have not been studied enough.

In this paper, we study the effects of laser polarization, in association with the transmittance, on shock generation and ion acceleration using particle-in-cell (PIC) simulations. One major result of our study is that the average and total energies of ions accelerated by a CP-driven shock are a couple of times higher than those accelerated by an LP-driven shock. This is partially due to the better ability of CP pulses in density compression even in relatively low plasma density, where the electrons are heated more easily due to the high transmittance, and, accordingly, the shock is faster than in high-density plasmas. In contrast, LP pulses, which are much less reflective than the CP pulses [24–26], require sufficiently high density of the plasma for density compression, where the shock is generally slow. Though the LP shock can still be generated even in low density, the shock potential in this case is usually too weak to reflect ions with high speed.

Another interesting point we found is that the transmittance is a singly dominant parameter for determining the CP-shock formation, while in the LP case, the shock formation is strongly affected by the rear side scale length as well as the transmittance. The shock formation in low-density plasma and independence on the target size are practical advantages of using CP pulses for shock under the limited controllability of the target conditions and moderate energy of driving pulses.

This paper is organized as follows. In Sec. II, we present the major results of one-dimensional (1D) simulations. Two-dimensional simulations regarding the polarization effects on transverse instability are presented in Sec. III. The conclusion is given in Sec. IV.
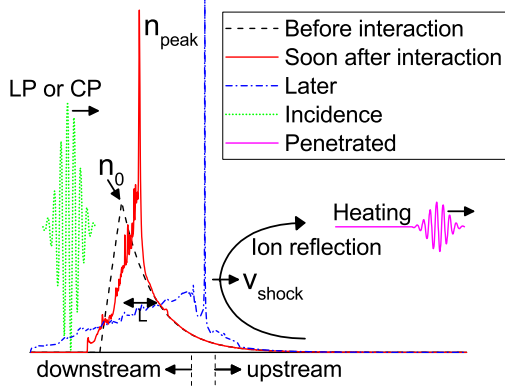
_____
*mshur@unist.ac.kr

FIG. 1. Schematic figure of the system. Initial plasma density has a linear ramp rising over 10 μm in the front and an exponentially falling profile with scale length L in the rear. When an ultrashort laser pulse propagates, the plasma density is compressed and some portion of the pulse energy penetrates through the compressed layer by relativistic transparency. The compressed density layer (shock) moves through the plasma even in the absence of a driving laser pulse, reflecting upstream ions with twice the velocity of the density layer, i.e., $\sim 2v_{\text{sh}}$.

II. ONE-DIMENSIONAL SIMULATIONS

Simulations were carried out using cplPIC (computational-plasma-lab Particle-In-Cell) [27,28], where the numerical dispersion-free field solver [29] was adopted. The 1D PIC simulations were conducted varying the peak initial density $n_0 = 3$–$10n_c$, and normalized field strength $a_0 = 10$–20 for different scale lengths of the plasma, i.e., $L = 5$, 10, and $15\,\mu$m.

The density of the plasma has a linearly rising ramp from 32 to 42 μm and an exponentially falling profile with scale length L in the rear. Use of such a plasma profile has been motivated by recent reports that the sheath field effect can be suppressed by the exponentially falling tail of the plasma density [7]. Gaussian pulse duration at full width at half maximum is 60 fs for LP pulses and 30 fs for CP pulses. By using different pulse durations for CP and LP, the total pulse energies and peak amplitude a_0 are kept the same for both polarizations. Simulation domain size is 300 μm, which is divided by 2.5-nm-long meshes. The number of simulation particles per cell per species is 200. The schematic of the system is illustrated in Fig. 1.

One major result of our one-dimensional simulations is that the total and average energies of reflected ions from the CP-driven shock are a couple of times larger than those from the LP-driven shock. In Figs. 2(a) and 2(b), the average energy and number of reflected (i.e., shock-accelerated) ions are presented for a wide range of initial plasma densities and $a_0 = 20, L = 15\,\mu$m. In averaging the ion energy, we excluded thermally expanding ions to consider purely reflected ions only, which are proportional to the shock speed. In the LP case [Fig. 2(a)], the maximum average energy of ions is approximately 350 MeV at a plasma density of $3n_c$–$5n_c$, while in the CP case, it is close to 800 MeV at a lower plasma density of around $2n_c$ [Fig. 2(b)].

Higher average ion energy indicates that the shock moves faster, since the velocity of reflected ions is approximately twice the shock speed. The larger shock speed in CP polarization, as compared to LP, originates from the different transmittance and ability of density compression (hole boring).
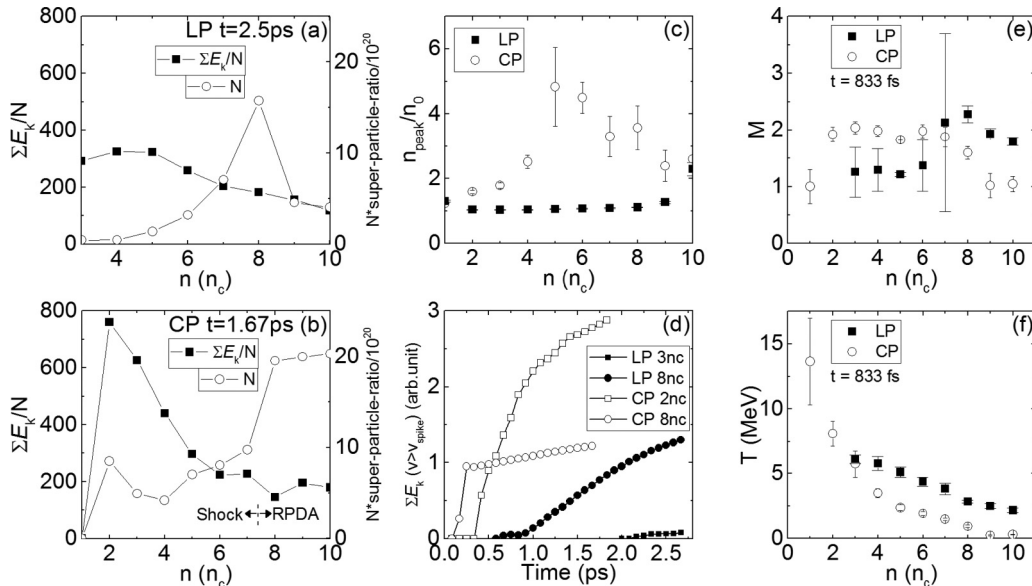

FIG. 2. Number (N) and average ($\sum \gamma mc^2/N$) energy of reflected ions from the shock for (a) an LP pulse and (b) a CP pulse. The rear scale length is L = 15 μm and the laser amplitude is $a_0 = 20$. (c) Ratio of the peak density of the compressed layer (n_{peak}) to the peak initial density n_0 measured after 80 fs from the time when the entire laser pulse passes through the position of the peak initial density ($x = 42\,\mu$m), corresponding to around 424 fs for LP and 322 fs for CP. The data were averaged over a 16-fs time interval. (d) Time evolution of the total energy ($\sum \gamma mc^2$) of reflected ions. (e) Time-averaged Mach number over a 16-fs interval around 833 fs, which is the time when the laser-plasma interaction ends. (f) Upstream temperature at 2–3 μm (order of Debye length) away from the compressed density layer, measured at the same time as the Mach number measurement. Error bars represent the standard deviation of the time average. The larger error cap corresponds to the LP data.

It is known that the Mach number of typical ion-reflecting ES shock is limited to $1.5 < M < 3.7$. Hence the sound speed $c_s = \sqrt{ZT_e/m_i}$ should be large in order to get a high speed shock, which requires strong electron heating. Another necessary condition is a fast-enough hole-boring speed to match the sound speed, so the compressed density layer from the hole-boring process is converted into the shock eventually. Previously, we revealed that the relativistically transmitting pulse energy is the major heating source in CP-driven shock [21]. In low-initial-density plasma, the transmittance is high and so is the sound speed. Simultaneously, the CP-driven hole-boring speed is also high in the low density, satisfying the conditions described above. However, this is not applicable to LP pulses, since they are generally more transparent than CP pulses under the same plasma condition, which prevents efficient momentum transfer to the plasma for density compression. The better ability of density compression by CP is well illustrated in Fig. 2(c), where the ratio of the peak compressed density n_{peak} to the peak initial density n_0 is presented. The LP pulse barely yields a compression ratio larger than unity until the initial density becomes high enough ($9n_c$), while it is larger than unity for most of the densities in the CP case. The practical meaning of this result is significant; as the CP shock is generated more efficiently in low-density plasmas, more controllable sources of overdense plasmas such as a gas-jet can be readily used in shock experiments. We note that the higher compression ratio is related more with the larger number of reflected (accelerated) ions, rather than with the higher ion energy. The ion energy is predominantly determined by the shock speed, which is usually faster in lower density. To avoid misleading, we also note that $n_{peak}/n_0 \sim 1$ in most of the LP cases and $n < 3n_c$ for CP [Fig. 2(c)] does not mean that the compression is weak. As the shock propagates in the upstream with downward density gradient, the ratio of the shock density to the background plasma density becomes large enough to reflect the background ions.

The higher transmittance of LP pulses leads also to the significantly delayed onset of the shock formation: As the compressed density is not as high as in CP, it should propagate a longer distance to reach the low-background-density region, where the contrast between the compression layer and the background plasma becomes just enough for shock generation. Figure 2(d) shows such a feature clearly: The total energy of the reflected ions from LP begins to rise long after the onset of CP-driven shock by several hundred femtoseconds, which is a time scale for the shock to propagate the entire target length.

The time-averaged Mach numbers of the compressed density layer driven by LP pulses [squares, Fig. 2(e)] satisfy the Mach number condition for ES shock for $n \geqslant 7n_c$, when they are measured at $t = 833$ fs (time when the laser-plasma interaction ends). In contrast, the compressed layer by CP pulses [circles, Fig. 2(e)] meets the Mach number condition for the low-density plasmas ($n \leqslant 7n_c$). Generally, the Mach number changes as the layer propagates under nonuniform density and temperature. For the particular case with $L = 15$ μm and $a_0 = 20$, we observed that the Mach number of the LP-driven layer eventually reached the proper range, even for the low densities. In the CP, however, the layer in the high-density cases ($n > 7n_c$) did not satisfy the shock condition until the end of simulations. The large error bar at
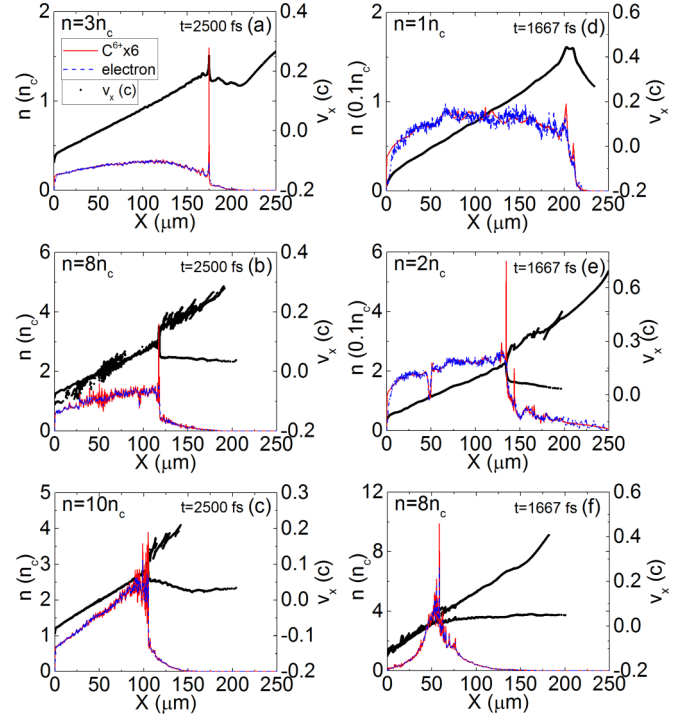

FIG. 3. Phase and density illustration when an LP pulse with $a_0 = 20$ impinges on (a) $n_0 = 3n_c$, (b) $n_0 = 8n_c$, and (c) $n_0 = 10n_c$ plasmas and a CP pulse with same intensity impinges on (d) $n_0 = 1n_c$, (e) $n_0 = 2n_c$, and (f) $n_0 = 8n_c$ plasmas. $L = 15$ μm for all cases.

$n = 7n_c$ in LP is related with the uncertainty in determining the position of the compression layer, which appears often during the conversion of the compressed layer to the shock. When the Mach number is measured later than $t = 833$ fs, the large error bar appears at $n = 6n_c$, while the case of $n = 7n_c$ enters the shock regime with its error bar being reduced. This feature is consistent with the delayed onset of the LP shock in low densities presented in Fig. 2(d).

Upstream temperature is illustrated in Fig. 2(f). The temperature of the LP-driven plasma in the high-density regime, where the LP shock is generated best, is lower than the CP-driven temperature in the low-density regime, where the CP-shock formation is efficient. Obviously, the high sound speed in the low density leads to faster CP-driven shocks than the LP-driven ones, leading to higher ion energy.

Figure 3 shows representative cases of ion phase portraits along with ion and electron densities. Figure 3(b) and 3(e) are the cases where the total energy of reflected ions is the maximum for LP and CP, respectively. In these cases, the velocity doubling by reflection on the shock front is clearly observed for both polarizations. For a very low density plasma ($n \sim n_c$) in the CP case [Fig. 3(d)], electron heating is strong due to the high transmittance, so thermal expansion is dominant in the acceleration process. High-density ($n > 7n_c$) plasma is opaque to the CP pulse, resulting in an radiation-pressure-acceleration (RPA)-dominant regime, which is characterized by cold plasma, Mach number not matching the ES-shock condition and ions being accelerated during the laser irradiation only; in addition, the ion phase space takes a typical shape of RPA regimes [Fig. 3(f)].
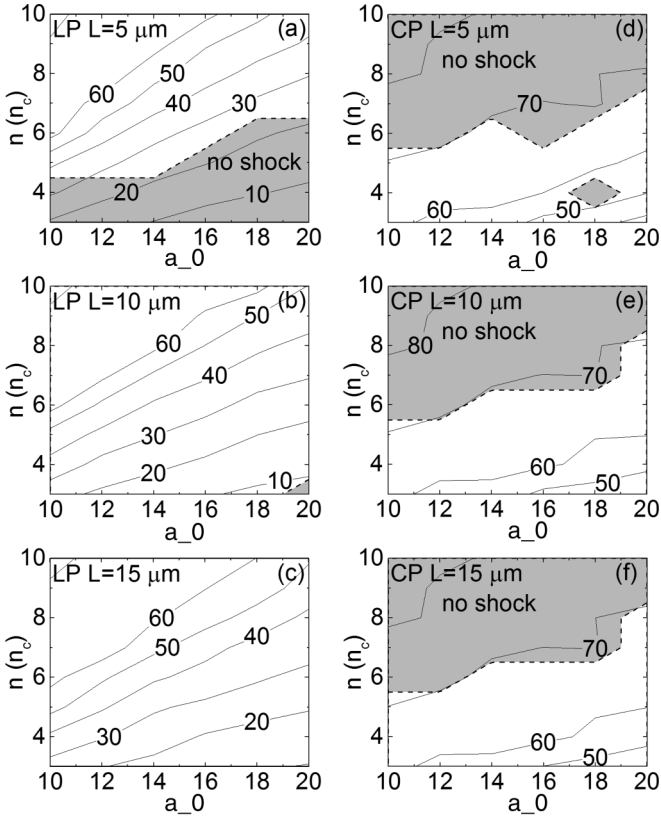
FIG. 4. Regime of shock formation and reflectance contour lines drawn on planes of n_0 and a_0 for different L's. Shock or no-shock by [(a)–(c)] an LP pulse and [(d)–(f)] by a CP pulse is determined at the same time as in Fig. 3.

The second major result of the 1D simulations is the observation that the shock formation by CP pulse is strongly correlated with the transmittance (T) only of the laser pulse. On the other hand, the rear scale length L of the plasma is an important parameter that influences the shock formation in LP cases. Figure 4 illustrates contour lines of reflectance ($R = 1 - T$) and the shock formation region in the a_0-n_0 plane for different L's. It was found that in CP cases, the boundary between the shock and no-shock regions is determined by a narrow range of reflectance, approximately from 60 to 80%, regardless of the rear scale length. This feature can be understood from the relation of transmittance and the hole-boring speed. Assuming a fraction η of the transmitted pulse energy is converted to the thermal energy of electrons, the temperature is estimated to be

$$k_B T_e \sim \eta T \frac{\epsilon_0 E_0^2}{n_0} = \eta T \frac{n_c}{n_0} m c^2 a_0^2, \qquad (1)$$

where E_0 is the electric field amplitude of the laser pulse and T is the transmittance. Hence the sound speed is estimated to be

$$\frac{c_s}{c} \sim \sqrt{\eta Z T \frac{n_c}{n_0} \frac{m}{m_i}} a_0, \qquad (2)$$

where m and m_i are the masses of electron and ion, respectively. For the parameter range considered in our simulations,

$\sqrt{\frac{n_c}{n_0} \frac{m}{m_i}} a_0 \ll 1$. Then the hole-boring speed [16,17,30] is approximated to be

$$\frac{v_{HB}}{c} = \frac{\sqrt{(1 - T/2) Z \frac{n_c}{n_0} \frac{m}{m_i}} a_0}{1 + \sqrt{(1 - T/2) Z \frac{n_c}{n_0} \frac{m}{m_i}} a_0} \sim \sqrt{\left(1 - \frac{T}{2}\right) Z \frac{n_c}{n_0} \frac{m}{m_i}} a_0. \qquad (3)$$

Since the Mach number of the ES shock should be within $M_{min} < M < M_{max}$, where $M_{min} \sim 1.5$ and $M_{max} \sim 3.7$, assuming the hole-boring speed is comparable to the shock speed, the minimum necessary transmittance is approximately

$$T > \frac{1}{\eta M_{max}^2 + 1}, \qquad (4)$$

which is, with $\eta \sim 0.17$, comparable to the 30% transmittance (i.e., 70% reflectance) observed from the simulations.

In LP cases, from the scaling laws of electron temperature in Refs. [31,32], $T_e \propto a_0$, leading to the sound speed proportional to $\sqrt{a_0}$. In the highly transparent regime we consider, Eq. (3) cannot be used to describe the hole-boring speed of LP. Instead, Eq. (1) in Ref. [24] can be used to describe the propagation speed of the density layer. Those scaling laws do not reduce to a simple equation of the Mach number depending on the transmittance only as in the CP cases. Moreover, the shock formation by LP strongly depends on the scale length L. As described by Figs. 2(c) and 2(d), the onset of an LP shock is significantly delayed due to weak density compression. During the delayed period, thermal expansion of the plasma becomes dominant in the rear side. Since the plasma expands faster in shorter rear length [19], the LP shock disappears when the scale length is too short. Figures 4(a)–4(c) show that the LP-shock generation correlates with the transmittance but is more strongly affected by the rear scale length. Note that weak dependence on target length L can be an advantage of CP shock, since the target length and density (or transmittance) can be used as independent control parameters of the shock formation.

Although our simulations do not cover the effects of pulse duration for different polarizations, a few general outcomes for longer pulse duration can be deduced. If the pulse duration of the LP pulse were increased, then the electron temperature would increase via reacceleration of hot electrons as described in Ref. [7]. Then the plasma density should also be increased to compensate for the enhanced transmittance due to the high temperature, as is done in Ref. [7] to maintain the shock generation. In contrast, the longer CP-pulse duration would have an opposite effect. A longer, gently rising pulse front is more effective in compressing the plasma [33]. High density of the compressed layer suppresses the transmittance of the CP pulse, thereby reducing the temperature. Considering a certain amount of transmittance is necessary for CP-driven shock, the CP would require lower plasma density for effective shock generation.

Another fair comparison of LP and CP can be done by having the LP amplitude be higher than the CP amplitude by a factor of $\sqrt{2}$, and keeping the same pulse duration, leading to the same relativistic mass correction in average for both polarizations. However, the transparency of LP with the same

a_0 is already higher than that of CP as presented in Fig. 4, because of the difference in compression ratio [Fig. 2(c)]. Increased a_0 of LP would lead to even larger transparency and temperature, which could possibly result in rapid destruction of the compressed layer in multidimensional situations.

III. TWO-DIMENSIONAL SIMULATIONS

When an ultraintense laser pulse impinges a near-critical density plasma in multidimensional systems, filaments of quasistatic magnetic field are generated on the irradiated surface due to Weibel instability [34,35]. The strong growth of filaments would destroy the compressed density layer required for shock formation. Furthermore, the hole-boring velocity is reduced by the instabilities because the laser pulse cannot transfer its momentum fully to the irradiated surface.

To identify the effects of the transverse-directional instabilities on shock formation by different polarizations, 2D simulations were conducted. In 2D simulations, lengths of the simulation domain and cell are $X = 250\,\mu m, Y = 60\,\mu m$, $dx = 5$ nm, and $dy = 20$ nm, respectively. The number of superparticles per cell per species is 20 at the peak initial density; the corresponding total number of superparticles is 2.7×10^8. Plasma and laser parameters are the same as those in 1D simulation. The spot size of a Gaussian laser pulse is $10\,\mu m$.

As Weibel instability is directly related to evolution of the magnetic field fluctuation, in Fig. 5, we measured the distribution of magnetic field B_z and ion density n_i at $t = 333$ fs for [Figs. 5(a) and 5(c)] LP and [Figs. 5(b) and 5(d)] CP pulses. In the LP case, the magnetic field intensity is 2 times higher than that caused by the CP pulse, as in Figs. 5(a) and 5(b). Due to the instability, the compressed density layer is deformed more severely by LP pulses. The larger fluctuation of B_z in LP than in CP can be explained by the strong longitudinal heating by LP pulses, which yield larger anisotropy of the electron temperature, thereby leading to faster growth of the transverse ripple of B_z from Weibel instability. The transverse magnetic
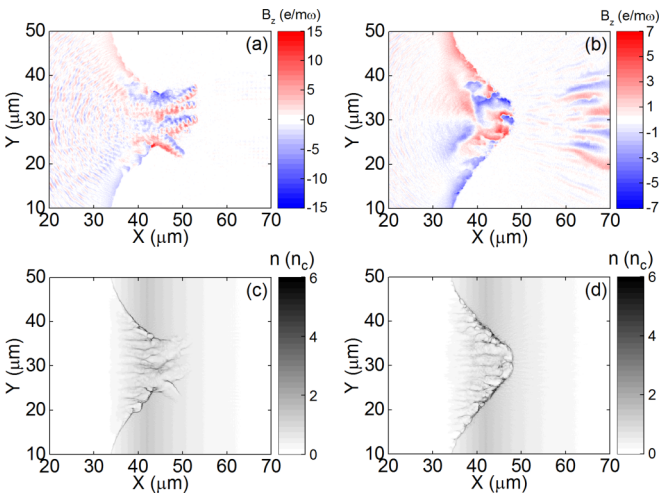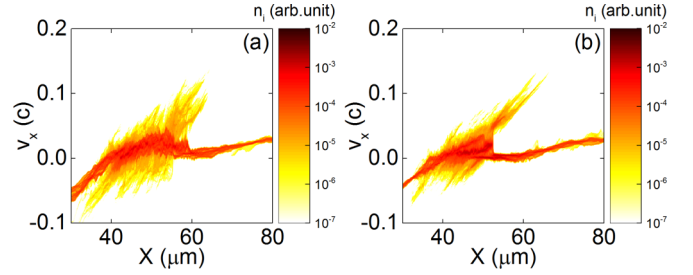

FIG. 6. Phase space of ions at $t = 800$ fs for (a) an LP pulse and (b) a CP pulse.

ripple induces the transverse modulation of the electron density. The laser field can leak through the low-density region of the modulated density, resulting in "holes" in B_z and density distribution [Figs. 5(a) and 5(c)]. In this case, there appear density filaments and channels, which the laser pulse is split into. In our parameters, three laser paths with different directions were observed, as in Fig. 5(a), and three minor shocks were formed along each path, whereas the filamentation is not so significant in the CP case, as in Figs. 5(b) and 5(d), leading to a large single, unidirectional shock formation.

From Fig. 6 it is clearly observed that ions reflected by the CP shock are concentrated within a narrow region in the x-u_x phase space, implying the velocity doubling is caused by a single shock front [Fig. 6(b)]. Meanwhile, the reflected ions in the LP case are spread with lower density over a wide region, which is the overlap of reflected ions from multiple minor shocks. The total energy of reflected ions $\sum E_{\rm ion}$ as a result of the CP shock at the laser axis is measured to be 1.5 times higher than the LP-shock ions. Note that for this calculation, reflected ions were selected within $52\,\mu m < X < 65\,\mu m$, $28\,\mu m < Y < 32\,\mu m$, and $0.046c < v_x$ at $t = 800$ fs. Those simulation results show that the CP is much less affected by Weibel instability than the LP, thus enabling efficient shock formation, even in a low-density regime. Behind the highly peaked ion population around the shock front, much lower density ions are scattered. The origin of those ions is attributed to the weak acceleration by the thermal sheath field.

IV. CONCLUSION

We investigated ES-shock formation in response to ultrashort LP and CP pulses using one- and two-dimensional PIC simulations. For both polarizations, efficient ES-shock formation and ion acceleration could be observed in semitransparent plasmas. When CP pulses are utilized, we found that the optimal plasma density for the high speed shock is much lower ($\sim 2n_c$) than that in the LP case ($\sim 8n_c$), and the onset of shock formation is markedly faster. Furthermore, the average and total energies of reflected ions are found to be a couple of times higher in CP than in LP. We also found that the transmittance is a singly dominant parameter to determine the CP shock formation, while the LP shock depends strongly on the rear side scale length. In two-dimensional simulations, CP pulses were found to effectively suppress the instabilities, resulting in more stable compression of the plasma layer and unidirectional single shock formation.

FIG. 5. Distribution of magnetic field B_z and ion density n_i at $t = 333$ fs when [(a) and (c)] an LP pulse impinges on $n_0 = 8n_c$ plasmas and [(b) and (d)] a CP pulse impinges on $n_0 = 8n_c$ plasmas. Magnetic field intensity and ion density were normalized.

ACKNOWLEDGMENTS

[1] A. Henig, S. Steinke, M. Schnürer, T. Sokollik, R. Hörlein, D. Kiefer, D. Jung, J. Schreiber, B. M. Hegelich, X. Q. Yan, J. Meyer-ter-Vehn, T. Tajima, P. V. Nickles, W. Sandner, and D. Habs, Phys. Rev. Lett. **103**, 245003 (2009).

[2] L. O. Silva, M. Marti, J. R. Davies, R. A. Fonseca, C. Ren, F. Tsung, and W. B. Mori, Phys. Rev. Lett. **92**, 015002 (2004).

[3] M. Chen, Z.-M. Sheng, Q.-L. Dong, M.-Q. He, S.-M. Weng, Y.-T. Li, and J. Zhang, Phys. Plasmas **14**, 113106 (2007).

[4] A. Macchi, A. S. Nindrayog, and F. Pegoraro, Phys. Rev. E **85**, 046402 (2012).

[5] H. Y. Wang, C. Lin, B. Liu, Z. M. Sheng, H. Y. Lu, W. J. Ma, J. H. Bin, J. Schreiber, X. T. He, J. E. Chen, M. Zepf, and X. Q. Yan, Phys. Rev. E **89**, 013107 (2014).

[6] A. Zhidkov, M. Uesaka, A. Sasaki, and H. Daido, Phys. Rev. Lett. **89**, 215002 (2002).

[7] F. Fiuza, A. Stockem, E. Boella, R. A. Fonseca, L. O. Silva, D. Haberberger, S. Tochitsky, C. Gong, W. B. Mori, and C. Joshi, Phys. Rev. Lett. **109**, 215001 (2012).

[8] D. Haberberger, S. Tochitsky, F. Fiuza, C. Gong, R. A. Fonseca, L. O. Silva, W. B. Mori, and C. Joshi, Nat. Phys. **8**, 95 (2012).

[9] M. Chen, Z.-M. Sheng, Q.-L. Dong, M.-Q. He, Y.-T. Li, M. A. Bari, and J. Zhang, Phys. Plasmas **14**, 053102 (2007).

[10] S. V. Bulanov, T. Zh. Esirkepov, V. S. Khoroshkov, A. V. Kuznetsov, and F. Pegoraro, Phys. Lett. A **299**, 240 (2002).

[11] E. Fourkal, I. Velchev, J. Fan, W. Luo, and C.-M. Ma, Med. Phys. **34**, 577 (2007).

[12] V. Malka, S. Fritzler, E. Lefebvre, E. d'Humières, R. Ferrand, G. Grillon, C. Albaret, S. Meyroneinc, J.-P. Chambaret, A. Antonetti, and D. Hulin, Med. Phys. **31**, 1587 (2004).

[13] P. McKenna, K. W. D. Ledingham, T. McCanny, R. P. Singhal, I. Spencer, M. I. K. Santala, F. N. Beg, K. Krushelnick, M. Tatarakis, M. S. Wei, E. L. Clark, R. J. Clarke, K. L. Lancaster, P. A. Norreys, K. Spohr, R. Chapman, and M. Zepf, Phys. Rev. Lett. **91**, 075006 (2003).

[14] M. Borghesi, A. Schiavi, D. H. Campbell, M. G. Haines, O. Willi, A. J. MacKinnon, L. A. Gizzi, M. Galimberti, R. J. Clarke, and H. Ruhl, Plasma Phys. Control. Fusion **43**, A267 (2001).

[15] D. W. Forslund and C. R. Shonk, Phys. Rev. Lett. **25**, 1699 (1970).

[16] A. P. L. Robinson, M. Zepf, S. Kar, R. G. Evans, and C. Bellei, New J. Phys. **10**, 013021 (2008).

[17] B. Qiao, S. Kar, M. Geissler, P. Gibbon, M. Zepf, and M. Borghesi, Phys. Rev. Lett. **108**, 115002 (2012).

[18] A. J. Mackinnon, Y. Sentoku, P. K. Patel, D. W. Price, S. Hatchett, M. H. Key, C. Andersen, R. Snavely, and R. R. Freeman, Phys. Rev. Lett. **88**, 215006 (2002).

[19] Y. Sentoku, T. E. Cowan, A. Kemp, and H. Ruhl, Phys. Plasmas **10**, 2009 (2003).

[20] O. Tresca, N. P. Dover, N. Cook, C. Maharjan, M. N. Polyanskiy, Z. Najmudin, P. Shkolnikov, and I. Pogorelsky, Phys. Rev. Lett. **115**, 094802 (2015).

[21] Y.-K. Kim, M.-H. Cho, H. S. Song, T. Y. Kang, H. J. Park, M. Y. Jung, and M. S. Hur, Phys. Rev. E **92**, 043102 (2015).

[22] H. Zhang, B. F. Shen, W. P. Wang, Y. Xu, Y. Q. Liu, X. Y. Liang, Y. X. Leng, R. X. Li, X. Q. Yan, J. E. Chen, and Z. Z. Xu, Phys. Plasmas **22**, 013113 (2015).

[23] Zs. Lecz and A. Andreev, Phys. Plasmas **22**, 043103 (2015).

[24] M. S. Hur, Y.-K. Kim, V. V. Kulagin, and H. Y. Suk, Laser Part. Beams **30**, 465 (2012).

[25] M. S. Hur, Y.-K. Kim, V. V. Kulagin, I. H. Nam, and H. Y. Suk, Phys. Plasmas **19**, 073114 (2012).

[26] M. S. Hur, V. V. Kulagin, and H. Y. Suk, Phys. Lett. A **379**, 700 (2015).

[27] M.-H. Cho, Y.-K. Kim, and M. S. Hur, Phys. Plasmas **20**, 093112 (2013).

[28] M.-H. Cho, Y.-K. Kim, and M. S. Hur, Appl. Phys. Lett. **104**, 141107 (2014).

[29] H.-C. Wu, arXiv:1104.3163.

[30] A. Macchi, F. Cattani, T. V. Liseykina, and F. Cornolti, Phys. Rev. Lett. **94**, 165003 (2005).

[31] A. Pukhov, Z.-M. Sheng, and J. Meyer-ter-Vehn, Phys. Plasmas **6**, 2847 (1999).

[32] S. C. Wilks, W. L. Kruer, M. Tabak, and A. B. Langdon, Phys. Rev. Lett. **69**, 1383 (1992).

[33] L. Ji, B. Shen, X. Zhang, F. Wang, Z. Jin, M. Wen, W. Wang, and J. Xu, Phys. Rev. Lett. **102**, 239501 (2009).

[34] X. M. Zhang, B. F. Shen, L. L. Ji, W. P. Wang, J. C. Xu, Y. H. Yu, and X. F. Wang, Phys. Plasmas **18**, 073101 (2011).

[35] Y. Sentoku, K. Mima, S. Kojima, and H. Ruhl, Phys. Plasmas **7**, 689 (2000).